Res Chem Intermed (2017) 43:5041–5054
DOI 10.1007/s11164-017-3038-9

Photo-generated conduction-band and shallow-trap electrons from UV irradiation on ethanol-adsorbed TiO_2 and N-TiO_2: an in situ infrared study

Jiawei Liu[1] · Long Zhang[1] · Xuesi Yao[1] · Steven S. C. Chuang[1]

Received: 15 April 2017 / Accepted: 16 May 2017 / Published online: 19 July 2017

Abstract The dynamic behaviors of conduction-band electrons (e^-_{CB}) and shallow-trap electrons (e^-_{ST}) generated from UV irradiation on ethanol-adsorbed TiO_2 and N-TiO_2 have been studied by in situ Fourier transform infrared spectroscopy (FTIR) in a diffuse reflectance mode at 300 K and 0.1 MPa. UV irradiation on ethanol-adsorbed TiO_2 resulted in the breaking of C–H bond of ethanol, the transfer of electrons from ethanol to the photo-generated holes on TiO_2 and N-TiO_2, the accumulation of e^-_{CB} and e^-_{ST}, and the formation of acetate on TiO_2 and the formation of acetate, formate, and formaldehyde on N-TiO_2. Accumulated e^-_{CB} and e^-_{ST} are manifested by broad and featureless IR absorbance spectra, which can be fitted into two models for estimation of their relative concentrations. N-doping onto TiO_2 produced a higher population of e^-_{ST} and generated e^-_{ST} and e^-_{CB} at a lower rate than TiO_2. The average energy level of e^-_{ST} was determined to be 0.30 eV for TiO_2 and 0.26 eV for N-TiO_2 below the conduction band. Upon terminating UV irradiation, the IR intensity of accumulated e^-_{CB} and e^-_{ST} showed a gradual decay in a time scale of minutes. This study demonstrated that the recombination of photo-generated electrons and holes can be a slow process on TiO_2 and N-TiO_2 in the presence of adsorbed ethanol under ambient conditions.

Special Issue of the 1st International Symposium on Photocatalysis at Fuzhou University.

✉ Steven S. C. Chuang
chuang@uakron.edu

[1] Department of Polymer Science, The University of Akron, Akron, OH 44325-3909, USA

Graphical Abstract

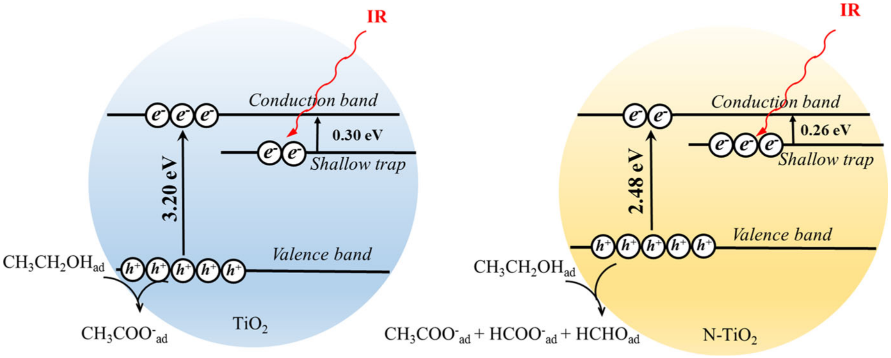

Keywords TiO_2 · N-doped TiO_2 · Conduction-band electrons · Shallow-trap electrons · Adsorbed ethanol · FTIR · Photocatalysis

Introduction

Photocatalysis involves light-induced generation of electron–hole pairs and transfer of electrons and holes to adsorbed species on the semiconductor catalyst surface [1–4]. The overall quantum efficiency of a photocatalysis process is governed by the rates of charge separation, interfacial charge transfer, trapping, and recombination [5–7]. Photo-generated electrons and holes must reach the catalyst surface sites to initiate the charge transfer reaction for converting the adsorbed reactants to products. Many photocatalytic reactions are limited by the rapid recombination of electrons and holes.

Although the time scales of photocatalytic steps range from femtoseconds to nanoseconds [8], the photo-generated electrons produced from adsorbed species can persist in TiO_2 for a long period of time at a scale of minutes to hours after terminating UV irradiation [9]. These long-life electrons, which do not get involved in either recombination with holes or transfer to the catalytic site, could stay in the conduction band and in the shallow/deep traps. The trapped electrons have been associated with Ti^{3+} of which optical and electrical properties are affected by its surrounding lattice [10].

Many studies on the generation and consumption of photo-generated electrons have been conducted at temperatures below 273 K and under vacuum [11–13], e.g., 90 K and 10^{-3} Pa vacuum which are not directly relevant to the working state of the photocatalyst. Thus, we have attempted to characterize the relative concentration of photo-generated electrons, conduction-band electrons, and shallow-trap electrons on TiO_2 and N-TiO_2 in the presence of adsorbed ethanol. Adsorbed ethanol is selected for this study because it possesses a high electron-donating potential and the structure of its adsorbed products has been well characterized [14]. N-TiO_2 is worthy of the investigation because of its visible light photocatalytic activity [15].

The objective of this study is to compare the rate of the generation and consumption as well as the relative concentration of e^-_{CB} and e^-_{ST} on TiO_2 and N-TiO_2 particles under typical conditions of photocatalysis (300 K, 0.1 MPa) using in situ IR spectroscopy. Experimental IR spectra, which were obtained as a function of time during UV irradiation, were fitted into two models, to obtain simulated IR intensities of e^-_{CB} and e^-_{ST}. N-doping onto TiO_2 increased the population of e^-_{ST} and decreased the rate of the generation of photo-generated electrons. The direct observation of the IR intensity of e^-_{CB} and e^-_{ST} under working state of photocatalysts will provide an in-depth insight into the role of various photo-generated charge carriers in photocatalysts.

Experimental

Materials preparation

P25 TiO_2 (Degussa), ammonia (NH_3, >99.98%, Praxair), and ethanol (99.5%, Fisher Scientific) were used as received. Nitrogen-doped TiO_2 (N-TiO_2) was prepared by treating P25 TiO_2 particles with ammonia (flow rate = 60 cm^3/min) at 723 K for 3 h.

Material characterization

Table 1 shows the characterization results of TiO_2 and N-TiO_2 catalysts. The nitrogen content of the N-TiO_2 catalyst was determined to be 5.4% (atomic ratio of N/Ti) by X-ray photoelectron spectroscopy (XPS) using PHI Versaprobe II scanning XPS microphobe with SmartSoft control package. The specific surface areas of P25 TiO_2 and N-TiO_2, measured by Micromeritics ASAP 2020 physisorption analyzer, were in the 40–50 m^2/g range. UV–Vis spectroscopic analysis (Hitachi U-3900 research grade UV–Vis spectrophotometer) gave the band-gap energy of TiO_2 and N-TiO_2 at 3.20 and 2.48 eV, respectively, which is consistent with literature values [16]. The last three columns show the fitting parameters used in this study, which will be discussed later.

Table 1 Properties of TiO_2 and N-TiO_2 photocatalysts

	N/Ti ratio	Band-gap (eV)	BET surface area (m^2/g)	Ethanol coverage (μmol/mg)	Fitting parameters of Eq. 2		Optical ionization energy of e^-_{ST} (eV)
					E_{DI} (eV)	E_{OP} (eV)	
TiO_2	N/A	3.20	49.7	820	0.06	0.12–0.35	0.30
N-TiO_2	5.4%	2.48	42.3	3780	0.06	0.12–0.35	0.26

In situ FTIR study

The experimental apparatus for in situ IR study is illustrated in Fig. 1 and consists of (1) a mass-flow controller (Brooks Instrument 5850), (2) a FTIR spectrometer equipped with a MCT detector (Nicolet 6700, Thermo Scientific), which accommodates a diffuse reflectance infrared Fourier transform spectroscopy (DRIFTS) cell (Harrick Scientific), and (3) a Hg lamp as UV light source (Oriel 6286) the intensity of which was set to 25 mW/cm^2. For each in situ IR study, 20 mg sample of TiO_2 or N-TiO_2 was loaded in a sample holder with 0.7 cm diameter and 0.2 cm depth, as shown in Fig. 1. The DRIFTS cell was capped by a three-window dome. Two of the windows in the IR beam path were ZnSe which is IR-transparent, while the third one was made of CaF_2 to allow the UV irradiation to pass through. TiO_2 and N-TiO_2 were exposed to an Ar/ethanol flow at a flow rate of 60 cm^3/min which was obtained by passing Ar flow through an ethanol saturator. Excess gaseous ethanol was purged out from the DRIFTS cell by flowing Ar for 20 min before the cell was switched to batch mode. IR spectra of the catalyst with adsorbed ethanol during UV irradiation were recorded as a function of time at a resolution of 4 cm^{-1} with four co-added scans. The IR spectra collected were presented in two forms: (1) the single beam (SB) spectrum, corresponding to a transmission spectrum, which was obtained by the Fourier transform of the IR interferogram; (2) absorbance (A) spectrum which was obtained by $A = -\log(I_t/I_0)$, where I_0 is the intensity of the background IR single beam spectrum of air and I_t is the intensity of the single beam spectrum collected at a specific time during UV irradiation.

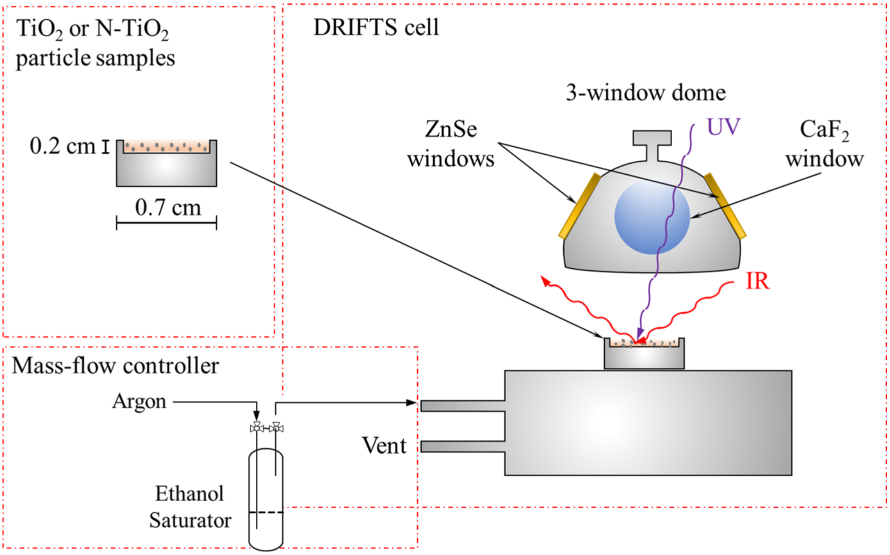

Fig. 1 Experimental setup for in situ IR study

Results and discussion

Simulated IR spectra of conduction-band and shallow-trap electrons produced from UV irradiation on ethanol-adsorbed TiO_2

Figure 2a presents single beam spectra obtained from pristine TiO_2 and TiO_2 with adsorbed ethanol before, during, and after UV irradiation; Fig. 2b shows the

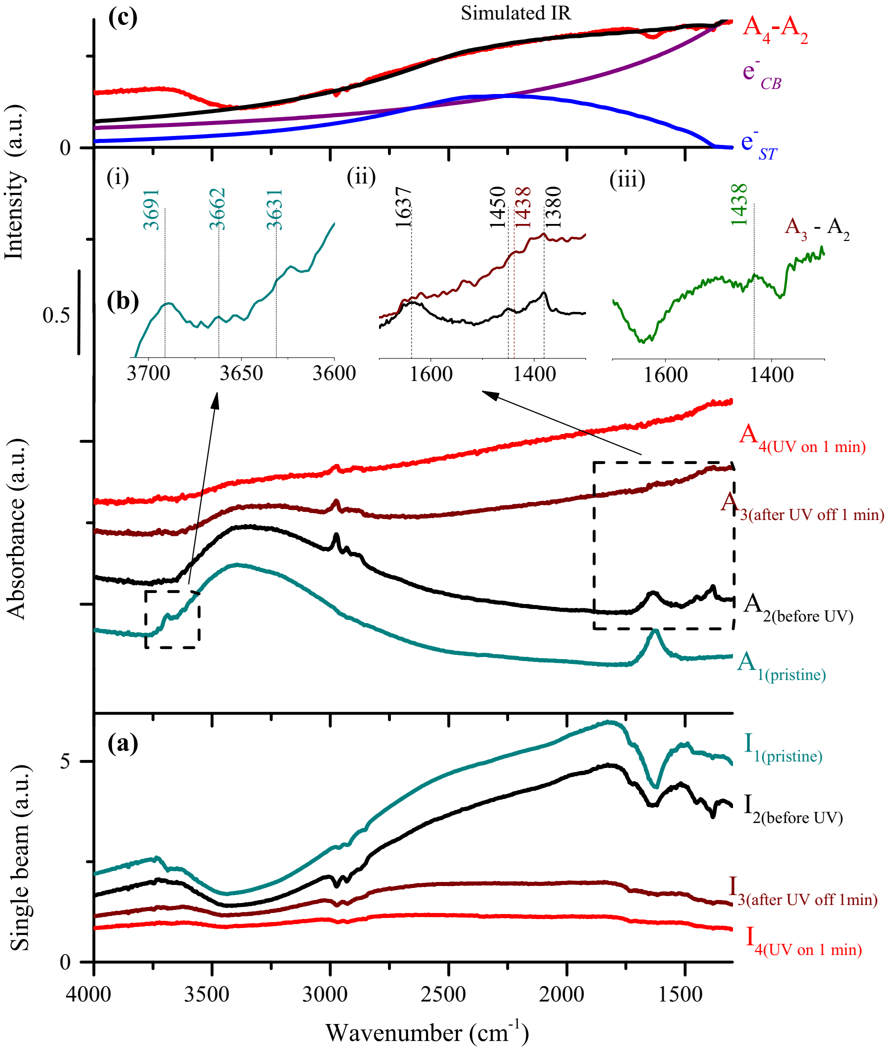

Fig. 2 **a** IR single beam spectra, **b** absorbance spectra of pristine TiO_2 sample and ethanol-adsorbed TiO_2 before, with, and after UV irradiation, and **c** simulated e^-_{CB} (*purple*), e^-_{ST} (*blue*), and IR (*black*) curves of the difference spectrum $A_4 - A_2$ (*red*). *Insets* (*i*) surface hydroxyls of pristine TiO_2; (*ii*) surface adsorbed species before and after UV irradiation; (*iii*) difference spectrum obtained from $A_3 - A_2$. (Color figure online)

corresponding absorbance spectra. The pristine TiO_2 sample gives a broad H_2O stretching at 3200–3700 cm^{-1} and a bending band at 1640 cm^{-1}. The insets in Fig. 2b show the surface hydroxyl groups of pristine TiO_2 sample and the adsorbed ethanol before and after the reaction, as well as the difference spectra between before and after UV irradiation. The assignments [14] of these various bands are listed in Table 2. The major IR-observable product generated after the UV irradiation is acetate at 1438 cm^{-1}. UV irradiation of TiO_2 with adsorbed ethanol resulted in an increase in the IR absorption which shows a nearly flat single beam spectrum in Fig. 2a and a featureless absorption spectrum in Fig. 2b. The featureless absorption spectrum is a result of the interactions of IR irradiation with shallow-trap electrons (e^-_{ST}) and conduction-band electrons (e^-_{CB}).

The specific effect of UV irradiation can be further highlighted by the difference spectrum $A_4 - A_2$ in Fig. 2c. To determine the contribution of e^-_{ST} and e^-_{CB} to the featureless difference spectra, we have adopted the following elaborated procedure [13] to obtain simulated e^-_{ST} and e^-_{CB} spectra using MATLAB.

(1) Smoothing the experimental IR spectrum with the Huber function to eliminate the outlying points in a curve. For example, the spikes and minor peaks are removed in this step for the following data fitting process.

(2) Obtaining the simulated e^-_{CB} spectrum by Eq. 1. The IR absorbance produced by the conduction-band electrons, ΔA_{CB}, can be described by the following:

$$\Delta A_{\mathrm{CB}} = A\tilde{v}^{-p} \tag{1}$$

where $\tilde{v}$ is the wavenumber, and p: is the scattering factor. The value of p for IR absorbance ranges from 1.5 to 1.7 [17]. $p = 1.7$ was found to give the best fit and was used to generate all simulated e^-_{CB} spectra.

(3) The simulated IR absorbance generated by e^-_{ST}, ΔA_{ST}, were obtained by Eq. 2 [13]:

Table 2 Band assignments of adsorbed surface species on TiO_2 and N-TiO_2

Wavenumber (cm^{-1})	Species	Vibrational mode
1380	$C_2H_5O_{ad}$	$\delta_s(CH_2)$
1438	$CH_3COO^-_{ad}$	$v_s(COO)$
1449	$C_2H_5O_{ad}$	$\delta_{as}(CH_2)$
1549	$CH_3COO^-_{ad}$	$v_{as}(COO)$
1577	$HCOO^-_{ad}$	$v_{as}(COO)$
1618	$HCHO_{ad}$	$v(C{=}O)$
1640	H_2O_{ad}	$\delta(OH)$
3633	Ti–OH (triple-bonded)	$v(OH)$
3663	Ti–OH (double-bonded)	$v(OH)$
3696	Ti–OH (linear)	$v(OH)$

$$\Delta A_{\mathrm{ST}} = A_0 \sum_{i=1}^{24} \alpha_i \frac{(E - E_{\mathrm{OP}}^i)^{1.5}}{E(E - E_{\mathrm{OP}}^i + E_{\mathrm{DI}})^4} \tag{2}$$

> where α: a weighting factor defining the contributions of the IR absorbance resulted from the shallow-trap electrons with different optical ionization energies, E_{OP}^i. E_{OP}^i: the optical ionization energy (i.e., the photon energy required to excite an electron from a trap). E_{DI}: the donor ionization energy (i.e., the thermal energy required to generate a carrier).

A set of values for these parameters in Table 1 were selected to obtain the best fit simulated IR absorbance curve. The *Eop* value, which corresponds to the energy level of the trapped electron, can be obtained from the maximum point of the simulated e_{ST}^- curve.

The simulated IR spectrum which was obtained from the summation of simulated e_{ST}^- and e_{CB}^- curves (shown in Fig. 2c), is a perfect match with experimental IR spectrum in the region of 1300–3300 cm^{-1}, which is the range of energy with most optical ionization.

Figure 3 shows the difference spectra of TiO_2 with adsorbed ethanol collected as a function of time upon UV irradiation. The difference spectrum at $t = 60$ s corresponds to A_4 in Fig. 2c.

Figure 3b, c show the evolution of the simulated e_{CB}^- and e_{ST}^- spectra resolved from difference spectra in Fig. 3a using Eqs. 1 and 2. The intensities of e_{CB}^- and e_{ST}^- absorption curves dramatically increased upon UV irradiation. The rate of increase slowed down after $t = 3$ s and then reached a plateau after around 12 s. These variations are plotted in Fig. 5 for comparison between TiO_2 and N-TiO_2.

The monotonic increase at the lower wavenumber region in e_{CB}^- spectra in Fig. 3b results from the Drude absorption of free electrons at the conduction band, which can be attributed to the intraband and interband transitions of the accumulated electrons [18, 19]. The peak (i.e., maxima) of the e_{ST}^- curves shifted from low to high wavenumber as their intensities grew, as shown in Fig. 3c. Higher wavenumbers of the peaks of e_{ST}^- curves correspond to higher IR photon energies which required to excite electrons from the shallow trap to conduction band.

Simulated IR spectra of conduction-band and shallow-trap electrons produced from UV irradiation on ethanol-adsorbed N-TiO_2

Figure 4 shows the IR spectra obtained from ethanol-adsorbed N-TiO_2 under UV irradiation. The spectra of pristine TiO_2 and N-TiO_2 in the region between 3550 and 3750 cm^{-1}, shown in Figs. 2b and 4b, were attributed to surface hydroxyl (–OH) groups: linear –OH at 3693 cm^{-1}, bridged (double-bonded) –OH at 3663 cm^{-1}, and triple-bonded –OH at 3633 cm^{-1} [6]. Table 3 compares the intensities of these bands in Figs. 2b and 4b and revealed that the N-doping increased the population of double- and triple-bonded OH, which may serve as the sites where ethanol adsorbed [20]. The IR features of these OH groups vanished upon ethanol adsorption. Comparison between the IR spectra of TiO_2 and N-TiO_2 shows that N-TiO_2 had a

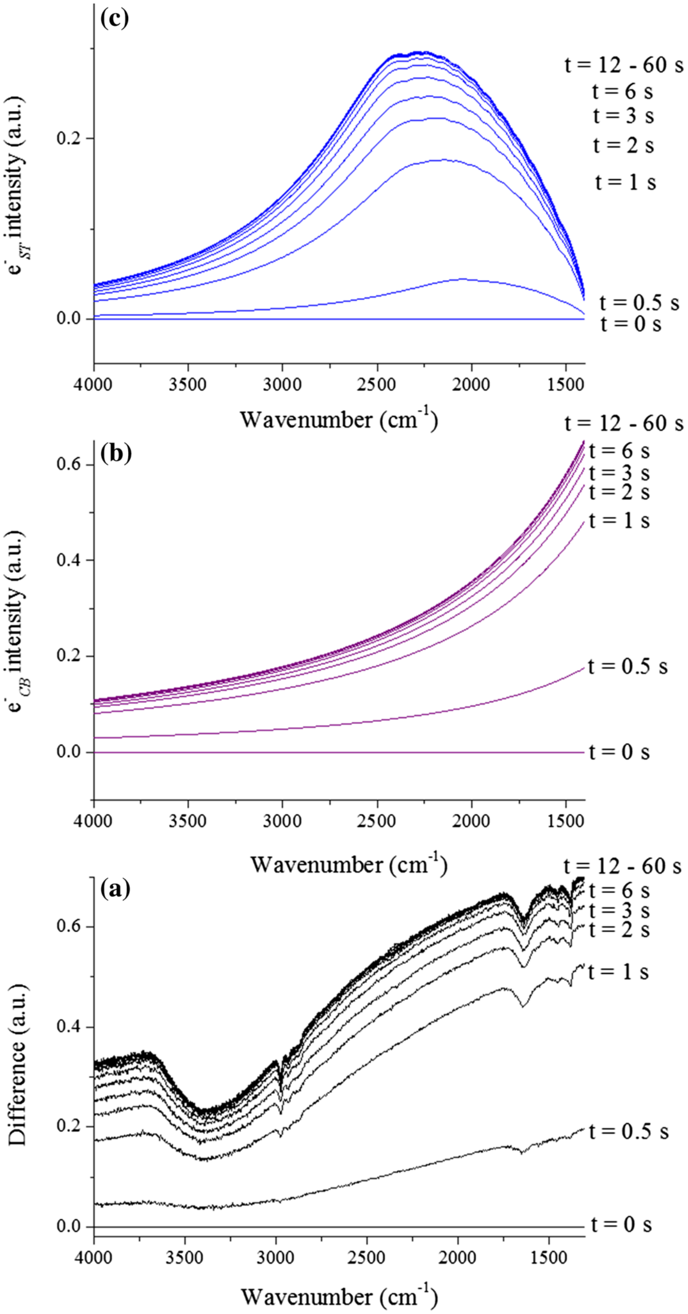

Fig. 3 **a** Difference spectra, **b** e^-_{CB} and **c** e^-_{ST} simulated absorption curves of ethanol-adsorbed TiO_2 during UV irradiation process

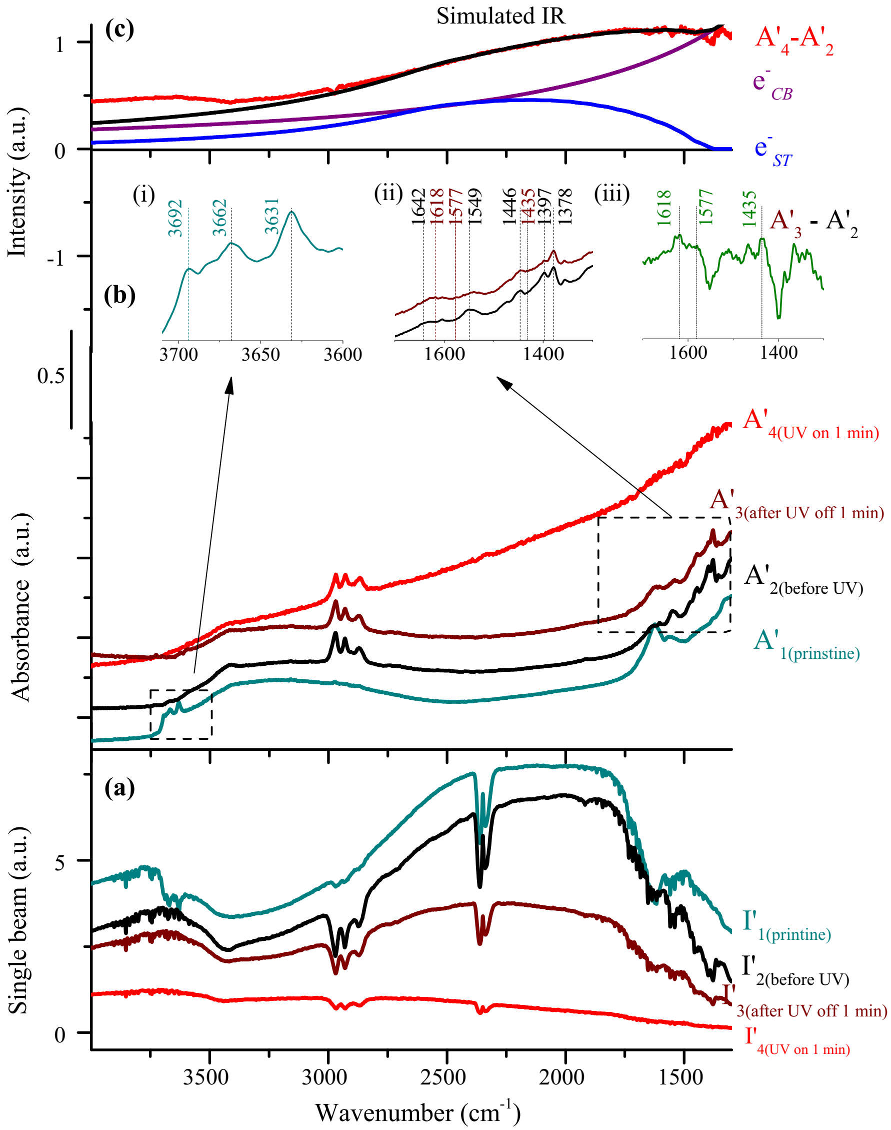

Fig. 4 **a** IR single beam spectra, **b** absorbance spectra of pristine N-TiO$_2$ sample and ethanol-adsorbed N-TiO$_2$ before, with, and after UV irradiation, and **c** simulated e^-_{CB} (*purple*), e^-_{ST} (*blue*), and IR (*black*) curves of the difference spectrum $A'_4 - A'_2$ (*red*). *Insets* (*i*) surface hydroxyls of pristine N-TiO$_2$; (*ii*) surface adsorbed species before and after UV irradiation; (*iii*) difference spectrum obtained from $A'_3 - A'_2$. (Color figure online)

higher intensity of C–H bonding in the range of 2800–3000 cm^{-1}, suggesting the presence of a higher coverage of ethanol on N-TiO$_2$. By calculating the ratio of the C–H peak areas of the two catalysts and comparing with the calibration results from our previous work [21], the ethanol coverage at room temperature was estimated to be 820 μmol/mg on TiO$_2$ and 3780 μmol/mg on N-TiO$_2$.

Table 3 Hydroxyl groups distribution on TiO_2 and N-TiO_2 samples

	Linear –OH ($3693\ cm^{-1}$) (%)	Double-bonded –OH ($3663\ cm^{-1}$) (%)	Triple-bonded –OH ($3633\ cm^{-1}$) (%)
TiO_2	54.3	19.6	26.1
N-TiO_2	31.0	33.3	39.7

Adsorbed ethanol on the surface of the photocatalysts at room temperature formed both molecularly adsorbed $CH_3CH_2OH_{ad}$ and dissociatively adsorbed $CH_3CH_2O_{ad}$ [22]. Although $CH_3CH_2OH_{ad}$ and $CH_3CH_2O_{ad}$ exhibited similar bands of C–H stretching vibrations at 2971 and 2931 cm^{-1}, their IR spectra in the region of 1000–1600 cm^{-1} exhibited different features. The most significant difference between TiO_2 and N-TiO_2 is that TiO_2 produced $CH_3COO^-_{ad}$ while N-TiO_2 produced three products, $CH_3COO^-_{ad}$, $HCOO^-_{ad}$, and $HCHO_{ad}$. The formation of $CH_3COO^-_{ad}$ from adsorbed ethanol can be considered as a key step for the injection of electrons from adsorbed ethanol to TiO_2/N-TiO_2, resulting in the accumulation of e^-_{CB} and e^-_{ST}.

$$CH_3CH_2OH_{ad} + nTiO_2 \rightarrow CH_3COO^-_{ad} + 3H^+ + 2e^- + nTiO_{(2-1/n)} \qquad (3)$$

The formation of proton has been verified by photo-oxidative degradation study of organics under aqueous condition [23]. $CH_3COO^-_{ad}$ may undergo further reactions to produce $HCOO^-_{ad}$ and $HCHO_{ad}$ as shown in our earlier studies [14].

Figure 5 shows the experimental IR absorbance, e^-_{ST} and e^-_{CB}'s intensity profiles over time and the relative distribution of e^-_{ST} and e^-_{CB} for TiO_2 and N-TiO_2. The experimental and simulated IR intensity profiles were taken at the IR intensity at 2000 cm^{-1} , which has been used as an index for the population of photo-generated electrons because they are usually not influenced by other bands related to ethanol [22]. High intensity ratio of e^-_{ST}/e^-_{CB} on N-TiO_2 suggests that our N-TiO_2 may contain more oxygen vacancies than TiO_2 because the shallow-trap band is known to be closely related to the oxygen vacancies in the TiO_2 structure [24].

The change of e^-_{CB} intensity led that of e^-_{ST} on both TiO_2 and N-TiO_2, supporting the previous proposed steps [25].

step (1) $\quad TiO_2 + hv \rightarrow e^-_{CB} + h^+_{VB}$

step (2) $\quad e^-_{CB} \rightarrow e^-_{\text{shallow trap with low } Eop}$

step (3) $\quad e^-_{CB} \rightarrow e^-_{\text{shallow trap with high } Eop}$

step (4) $\quad e^-_{trap} + h^+ \rightarrow \text{annihilation} + \text{heat}$

e^-_{CB} produced from UV irradiation was transferred to shallow trap sites, shown in step (2). Step (2) occurred at the first second after UV irradiation. After the first

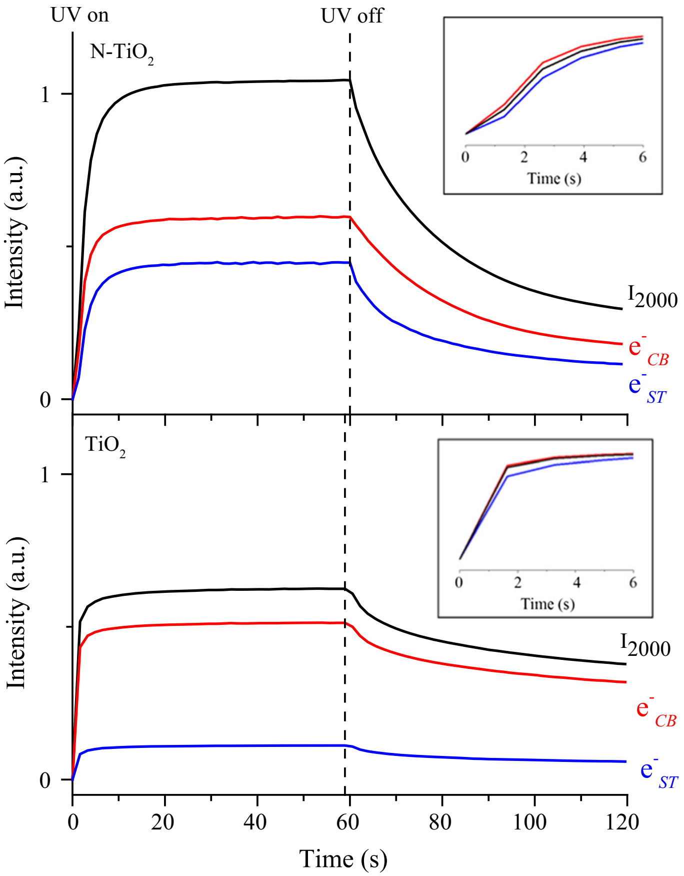

Fig. 5 The intensity of I_{2000}, e^-_{CB} and e^-_{ST} as a function of UV irradiation time for ethanol-adsorbed TiO_2 and N-TiO_2 (*insets* show the normalized rate of change in the first 6 s)

second, the step (3) began dominating as indicated by the shifting of the peak of the e^-_{ST} curves to high wavenumber (i.e., high optical ionization energy). The optical ionization energy for both TiO_2 and N-TiO_2 are plotted in Fig. 6 for comparison [25]. Termination of UV irradiation led to the decay of e^-_{CB} and e^-_{ST} curves, indicating the rate of charge carrier (e^- and h^+) recombination is higher than their generation. The decay curves levelled off after 120 s and did not return to the base line, indicating the accumulation of e^-_{CB} and e^-_{ST} and the long lifetime of electrons in the existence of ethanol.

Table 4 summarizes a number of related studies that were carried out under vacuum or aqueous conditions. These results showed accumulated e^-_{CB} and e^-_{ST} can persist for a long period of time. Our studies showed the accumulated e^-_{CB} and e^-_{ST} can co-exist with adsorbed ethanol and their products for a long period of time at 0.1 MPa and 300 K. The negative charges of accumulated e^-_{CB} and e^-_{ST} could be

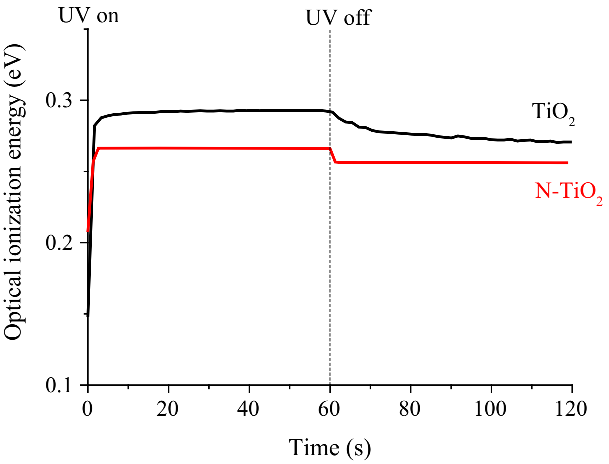

Fig. 6 The optical ionization energy of e^-_{ST} as a function of UV irradiation time

Table 4 Comparison of experimental techniques and conditions used in this field

Technique	Sample	Condition	Comments
Thermoluminescence and thermally stimulated currents	TiO_2 crystal (1 mm thickness)	90–160 K	Filling of traps increased lifetime of electrons [12]
Electron paramagnetic resonance (EPR)	TiO_2 particle	90 K, 10^{-3} Pa	Trapped electrons persist longer than 5 h at 90 K; major fraction of photo-excited electrons remain in the conduction band [11]
Attenuated total reflectance (ATR)	TiO_2 film (1 µm thickness)	Aqueous	e^-_{ST} and e^-_{CB} persist for hours [26]
Transmission-IR	TiO_2 particle	77 K, 10^{-6} Pa	Organic hole scavenger increases the lifetime of photo generated electrons to hours [13]
DRIFTS (this work)	Photocatalysts in various forms, including particle, film, liquid, etc.	Ambient or any desired conditions	e^-_{ST} has shorter lifetime than e^-_{CB}

balanced by protons on TiO_2 and N-TiO_2 of which sites for combination of H^+ and e^-_{CB}/e^-_{ST} may be blocked by adsorbed ethanol and its products.

The rise and fall of the IR intensity of e^-_{CB} and e^-_{ST} reflect their relative generation and consumption rates. The presence of high coverage of H_2O inhibited accumulation of both e^-_{CB} and e^-_{ST} on adsorbed ethanol on TiO_2 [14]. H_2O could shift the oxidation of adsorbed ethanol from a hole-initiated reaction to an electron-initiated reaction, resulting in a high rate of consumption of photo-generated electrons. These photo-generated electrons can be consumed by exposing to oxygen at a high rate, evidenced by a sharp decrease in their IR intensity [9]. The results of these studies suggest that photo-generated electrons are readily accessible to specific reactants. The key fundamental issue for the future study is identification of active sites where the transfer of e^-_{CB} and e^-_{ST} to adsorbed reactants occur.

Conclusions

Dynamic behaviors of photo-generated e^-_{CB} and e^-_{ST} on TiO_2 and N-TiO_2 have been studied by fitting experimental IR spectra to simulated IR curves of e^-_{CB} and e^-_{ST} at 300 K and 0.1 MPa. N-doping on TiO_2 produced a higher population of e^-_{ST} and generated e^-_{ST} and e^-_{CB} at a lower rate than TiO_2. The rise of e^-_{CB} curve leads that of e^-_{ST}, indicating e^-_{CB} is produced prior to e^-_{ST}. This observation further suggests that the trapped electrons were produced by the injection of e^-_{CB} to the trapped sites. Upon UV irradiation, e^-_{CB} filled in the trap sites of which energy levels are closer to the conduction band first and then fill in those farther away. Under constant UV irradiation, the average energy level of e^-_{ST} was determined to be 0.30 eV for TiO_2 and 0.26 eV for N-TiO_2 below conduction band. Upon terminating UV irradiation, the IR intensity of accumulated e^-_{CB} and e^-_{ST} at trap sites showed a gradual decay in a time scale of minutes. This study showed that the photo-generated electrons and holes can exist at a time scale of minutes in TiO_2 and N-TiO_2 in the presence of adsorbed ethanol under ambient conditions. To expand the practical applications of TiO_2-based materials, the investigations on the specific roles of e^-_{CB} and e^-_{ST} in photocatalysis are warranted.

Acknowledgements This work was supported by the University of Akron Polymer Science Faculty Initiation Fund. The authors thank Ms. Jie Yu and Mr. P. Patanapaniswa for valuable discussions.

References

1. J. Schneider, M. Matsuoka, M. Takeuchi, J. Zhang, Y. Horiuchi, M. Anpo, D.W. Bahnemann, Understanding TiO_2 photocatalysis: mechanisms and materials. Chem. Rev. **114**(19), 9919–9986 (2014)
2. M. Anpo, Photocatalysis on small particle TiO_2 catalysts. reaction intermediates and reaction mechanisms. Res. Chem. Intermed. **11**(1), 67 (1989)
3. M.R. Hoffmann, S.T. Martin, W. Choi, D.W. Bahnemann, Environmental applications of semiconductor photocatalysis. Chem. Rev. **95**(1), 69–96 (1995)
4. A.L. Linsebigler, G. Lu, J.T. Yates, Photocatalysis on TiO_2 surfaces: principles, mechanisms, and selected results. Chem. Rev. **95**(3), 735–758 (1995)
5. M. Anpo, Utilization of TiO_2 photocatalysts in green chemistry. Pure Appl. Chem. **72**, 1265 (2000)
6. R. Daghrir, P. Drogui, D. Robert, Modified TiO_2 for environmental photocatalytic applications: a review. Ind. Eng. Chem. Res. **52**(10), 3581–3599 (2013)
7. M. Yan, F. Chen, J. Zhang, M. Anpo, Preparation of controllable crystalline titania and study on the photocatalytic properties. J. Phys. Chem. B **109**(18), 8673–8678 (2005)
8. A. Yamakata, T. Ishibashi, H. Onishi, Kinetics of the photocatalytic water-splitting reaction on TiO_2 and Pt/TiO_2 studied by time-resolved infrared absorption spectroscopy. J. Mol. Catal. A Chem. **199**(1–2), 85–94 (2003)
9. F. Guzman, S.S.C. Chuang, Tracing the reaction steps involving oxygen and IR observable species in ethanol photocatalytic oxidation on TiO_2. J. Am. Chem. Soc. **132**(5), 1502–1503 (2010)

10. F. Amano, M. Nakata, A. Yamamoto, T. Tanaka, Effect of Ti^{3+} ions and conduction band electrons on photocatalytic and photoelectrochemical activity of rutile titania for water oxidation. J. Phys. Chem. C **120**(12), 6467–6474 (2016)
11. T. Berger, M. Sterrer, O. Diwald, E. Knoezinger, D. Panayotov, T.L. Thompson, J.T. Yates Jr., Light-induced charge separation in anatase TiO_2 particles. J. Phys. Chem. B **109**(13), 6061–6068 (2005)
12. A.K. Ghosh, F.G. Wakim, R.R. Addiss, Photoelectronic processes in rutile. Phys. Rev. **184**(3), 979–988 (1969)
13. D.A. Panayotov, S.P. Burrows, J.R. Morris, Infrared spectroscopic studies of conduction band and trapped electrons in UV-photoexcited, H-atom n-doped, and thermally reduced TiO_2. J. Phys. Chem. C **116**(7), 4535–4544 (2012)
14. Z. Yu, S.S.C. Chuang, In situ IR study of adsorbed species and photogenerated electrons during photocatalytic oxidation of ethanol on TiO_2. J. Catal. **246**(1), 118–126 (2007)
15. Y. Cong, J. Zhang, F. Chen, M. Anpo, Synthesis and characterization of nitrogen-doped TiO_2 nanophotocatalyst with high visible light activity. J. Phys. Chem. C **111**(19), 6976–6982 (2007)
16. A. Samokhvalov, Hydrogen by photocatalysis with nitrogen codoped titanium dioxide. Renew. Sustain. Energy Rev. **72**, 981–1000 (2017)
17. H. Zhao, Q. Zhang, Y.-X. Weng, Deep Surface trap filling by photoinduced carriers and interparticle electron transport observed in TiO_2 nanocrystalline film with time-resolved visible and mid-IR transient spectroscopies. J. Phys. Chem. C **111**(9), 3762–3769 (2007)
18. T. Berger, J.A. Anta, V. Morales-Flórez, Electrons in the band gap: spectroscopic characterization of anatase TiO_2 nanocrystal electrodes under fermi level control. J. Phys. Chem. C **116**(21), 11444–11455 (2012)
19. G. Boschloo, D. Fitzmaurice, Electron accumulation in nanostructured TiO_2 (anatase) electrodes. J. Phys. Chem. B **103**(37), 7860–7868 (1999)
20. H. Lin, J. Long, Q. Gu, W. Zhang, R. Ruan, Z. Li, X. Wang, In situ IR study of surface hydroxyl species of dehydrated TiO_2: towards understanding pivotal surface processes of TiO_2 photocatalytic oxidation of toluene. Phys. Chem. Chem. Phys. **14**(26), 9468–9474 (2012)
21. M. Ghosh, M. Lohrasbi, S.S.C. Chuang, S.C. Jana, Mesoporous titanium dioxide nanofibers with a significantly enhanced photocatalytic activity. ChemCatChem **8**(15), 2525–2535 (2016)
22. A. Rismanchian, Y.-W. Chen, S.S.C. Chuang, In situ infrared study of photoreaction of ethanol on Au and Ag/TiO_2. Catal. Today **264**, 16–22 (2016)
23. E. Pelizzetti, C. Minero, Mechanism of the photo-oxidative degradation of organic pollutants over TiO_2 particles. Electrochim. Acta **38**(1), 47–55 (1993)
24. G. Mattioli, F. Filippone, P. Alippi, A. Amore Bonapasta, Ab initio study of the electronic states induced by oxygen vacancies in rutile and anatase TiO_2. Phys. Rev. B **78**(24), 241201 (2008)
25. S.H. Szczepankiewicz, J.A. Moss, M.R. Hoffmann, Electron traps and the stark effect on hydroxylated titania photocatalysts. J. Phys. Chem. B **106**(31), 7654–7658 (2002)
26. D.M. Savory, A.J. McQuillan, IR spectroscopic behavior of polaronic trapped electrons in TiO_2 under aqueous photocatalytic conditions. J. Phys. Chem. C **118**(25), 13680–13692 (2014)